

---

# Study of Inhomogeneous Phases in the Walecka Model

---

Untersuchung von Inhomogenen Phasen im Walecka Modell

Bachelor-Thesis von Marco Schramm

December 10



TECHNISCHE  
UNIVERSITÄT  
DARMSTADT

Fachbereich Physik  
Institut für Kernphysik  
NHQ

Study of Inhomogeneous Phases in the Walecka Model  
Untersuchung von Inhomogenen Phasen im Walecka Modell

Vorgelegte Bachelor-Thesis von Marco Schramm

1. Gutachten: Prof. Dr. Jochen Wambach
2. Gutachten: PD Dr. Michael Buballa

Tag der Einreichung:

---

## Abstract

---

The focus of this thesis is on thermodynamic calculations in nuclear matter in general and the examination of inhomogeneous phases in particular. To describe nuclear matter we use the so called the Walecka model, which describes nuclear forces by the exchange of two mesons. We draw a phase diagram of nuclear matter and derive different thermodynamic observables. We also explain the existence of the first order phase transition by the behavior of the thermodynamic potential. We allow spatially dependent masses and find inhomogeneous phases for the case without vector interaction. We end with a qualitative discussion of the inhomogeneous phase diagram with vector interaction.

---

## Contents

---

<b>1</b>	<b>Introduction</b>	<b>3</b>
<b>2</b>	<b>The Walecka Model</b>	<b>4</b>
2.1	Limits for $T \rightarrow 0$ . . . . .	6
<b>3</b>	<b>Determination of the Coupling Constants</b>	<b>8</b>
<b>4</b>	<b>Homogeneous Phase Diagram</b>	<b>9</b>
<b>5</b>	<b>Inhomogeneous Phase</b>	<b>11</b>
5.1	Grand Canonical Potential . . . . .	11
5.1.1	Limits . . . . .	12
<b>6</b>	<b>Phase Diagram with Inhomogeneous Phases</b>	<b>14</b>
<b>7</b>	<b>Conclusion and Outlook</b>	<b>17</b>

---

## 1 Introduction

---

The first ideas of nuclear physics came up in the beginning of the 20th century. The first scattering experiments with  $\alpha$  particles by Ernest Rutherford 1909 showed that atoms consist of a nucleus and an electron cloud around it. From thereon the grasp for nuclei evolved and led to the discovery of the neutron in 1932. In 1935 Bethe and Weizsäcker developed their semi-empiric mass formula, which allows to calculate the mass of a nucleus by the knowledge of its constituents, the protons and neutrons. This led to the development of the liquid drop model by Niels Bohr in 1936. It describes nuclei as a fluid of nucleons, which interact by a strong nuclear force.

In this thesis we want to concentrate on nuclear matter, which means we consider only symmetric matter ( $N=Z$ ), neglect the Coulomb repulsion between protons and inspect very large volume and particle numbers, so the surface effects are small and don't have to be considered.

To describe highly condensed nuclear matter we use the Walecka model, that was developed by J. D. Walecka in 1973. It was one of the first relativistic approaches to the problem and can therefore describe some properties of nuclear matter that were not reproducible with non-relativistic models. The model uses baryon fields to describe the nucleons and two neutral isospin scalar mesons, a spin scalar  $\sigma$  meson and a spin vector  $\omega$  meson, to transmit nuclear forces.

Inhomogeneous phases have been investigated in the NJL model extensively, see for example [Nic09] and [CNB10]. The Walecka model is quite similar to the NJL model, so our aim is it to investigate the phase diagram for inhomogeneous phases in the Walecka model.

---

## 2 The Walecka Model

---

The Walecka model, or  $\sigma - \omega$  model is a relativistic mean-field theory to describe highly condensed nuclear matter. It was introduced by J.D. Walecka in 1973 [Wal74]. Our aim is to derive thermodynamical observables to calculate properties of nuclear matter as a many body system. This is done by introducing a mean field approximation for the meson fields, which act as exchange particles for the nuclear forces. Then we derive the grand canonical partition function which is needed to calculate the grand canonical potential, from which all other observables can be derived.

The Walecka model uses two mesons as exchange particles, the scalar  $\sigma$  meson and the vector  $\omega$  meson. The coupling constants  $g_\sigma$  and  $g_\omega$  are unknown and have to be determined by known properties of nuclei. Another problem is that the mass of the  $\sigma$ -meson cannot be determined very precisely, the literature only gives ranges  $m_\sigma = 400 - 1200$  MeV [N<sup>+</sup>10].

The Lagrangian density is given by

$$\mathcal{L}_W = \bar{\psi} \left[ i\gamma_\mu (\partial^\mu + ig_\omega \omega^\mu) - (m_0 - g_\sigma \sigma) \right] \psi + \frac{1}{2} (\partial_\mu \sigma \partial^\mu \sigma - m_\sigma^2 \sigma^2) - \frac{1}{4} \omega_{\mu\nu} \omega^{\mu\nu} + \frac{1}{2} m_\omega^2 \omega_\mu \omega^\mu. \quad (2.1)$$

This describes four particles, the two nucleons ( $\psi$ ), the scalar meson ( $\sigma$ ) and the vector meson ( $\omega$ ), with the following properties

Particle	Mass /MeV	Spin	Isospin
p	938.272	1/2	1/2
n	939.566	1/2	1/2
$\sigma$	400-1200	0	0
$\omega$	782.65	1	0

[N<sup>+</sup>10]

In this thesis we concentrate on isospin symmetric matter with  $m_0 = (m_n + m_p)/2 \approx 939$  MeV.

The first part in (2.1) describes the free nucleon and the nucleon-meson interaction, the second part is the free  $\sigma$ -meson and the third part is the free  $\omega$ -meson.

From the Lagrange density we get the following coupled Euler-Lagrange equations for the nucleons, the  $\sigma$  meson and the  $\omega$  meson

$$\left[ i\gamma_\mu (\partial^\mu - g_\omega \omega^\mu(x)) - (m_0 - g_\sigma \sigma(x)) \right] \psi(x) = 0, \quad (2.2)$$

$$(\square + m_\sigma^2) \sigma(x) = g_\sigma \bar{\psi}(x) \psi(x), \quad (2.3)$$

$$(\square + m_\omega^2) \omega_\mu(x) - \partial_\mu \partial^\nu \omega_\nu(x) = g_\omega \bar{\psi}(x) \gamma_\mu \psi(x). \quad (2.4)$$

To simplify the problem described above, we introduce a mean-field approximation. The meson fields and the nuclear currents are replaced by their mean values, which are spatially and time independent. We also split (2.4) into the time and the spatial parts of the four component vector. The Euler Lagrange equations (2.3) and (2.4) transform to

$$m_\sigma^2 \sigma = g_\sigma \langle \bar{\psi} \psi \rangle, \quad (2.5)$$

$$m_\omega^2 \omega_0 = g_\omega \langle \psi^\dagger \psi \rangle, \quad (2.6)$$

$$m_\omega^2 \omega_k = g_\omega \langle \bar{\psi} \gamma_k \psi \rangle = 0. \quad (2.7)$$

The expectation value  $\langle \bar{\psi} \gamma_k \psi \rangle$  in equation (2.7) equals zero due to rotational invariance. Now these average values can be plugged into equation (2.1) to obtain the mean-field Lagrangian

$$\begin{aligned} \mathcal{L}_{MF} = & \bar{\psi} \left[ i\gamma_\mu \partial^\mu - \gamma_0 \left( \frac{g_\omega}{m_\omega} \right)^2 \langle \psi^\dagger \psi \rangle - \left( m_0 - \left( \frac{g_\sigma}{m_\sigma} \right)^2 \langle \bar{\psi} \psi \rangle \right) \right] \psi \\ & - \frac{1}{2} \left( \frac{g_\sigma}{m_\sigma} \right)^2 \langle \bar{\psi} \psi \rangle^2 + \frac{1}{2} \left( \frac{g_\omega}{m_\omega} \right)^2 \langle \psi^\dagger \psi \rangle^2. \end{aligned} \quad (2.8)$$

In the further parts we express the coupling constants as  $G_S = \frac{1}{2} \left( \frac{g_\sigma}{m_\sigma} \right)^2$  and  $G_V = \frac{1}{2} \left( \frac{g_\omega}{m_\omega} \right)^2$ . We want to introduce the grand canonical partition function

$$Z = \text{Tr} e^{-\frac{1}{T}(\hat{H} - \mu \hat{N})}. \quad (2.9)$$

It is one of the most important quantities in statistical physics, as all thermodynamic observables can be derived from it. Here  $\hat{H}$  is the Hamiltonian,  $\hat{N}$  is the particle number operator and  $\mu$  is the chemical potential. This leads to the grand canonical potential

$$\Omega = -\frac{T}{V} \ln(Z). \quad (2.10)$$

To evaluate equations (2.9) and (2.10) we have to calculate the function

$$\exp \left( i \int_0^{1/T} d\tau \int_V d^3\vec{x} (\mathcal{L} + \mu \psi^\dagger \psi) \right) \quad (2.11)$$

with the imaginary time formalism, described in detail in [Kap05]. This allows us to define a combined Lagrangian

$$\tilde{\mathcal{L}} = \mathcal{L}_{MF} + \mu \psi^\dagger \psi. \quad (2.12)$$

We introduce the substitutions

$$M = m_0 - 2 \cdot G_S \langle \bar{\psi} \psi \rangle, \quad (2.13)$$

$$\tilde{\mu} = \mu - 2 \cdot G_V \langle \psi^\dagger \psi \rangle, \quad (2.14)$$

which correspond to a shifted mass and a shifted chemical potential. We can rewrite the combined Lagrangian

$$\tilde{\mathcal{L}} = \bar{\psi} \left[ i\gamma_\mu \partial^\mu + \gamma_0 \tilde{\mu} - M \right] \psi - G_S \langle \bar{\psi} \psi \rangle^2 + G_V \langle \psi^\dagger \psi \rangle^2. \quad (2.15)$$

For later discussions it is noteworthy that this Lagrangian looks similar to the mean-field Lagrangian of the Nambu-Jona-Lasino model (NJL). [Sch07]

The first part in equation (2.15) equals a free Lagrangian for a particle with mass  $M$  and chemical potential  $\tilde{\mu}$ . For this case the thermodynamic potential is well known [Kap05] and can be expressed as

$$\omega_F = -\frac{2}{\pi^2} \int_0^\infty dk k^2 \cdot \left[ T \cdot \ln \left( 1 + \exp \left( -\frac{E - \tilde{\mu}}{T} \right) \right) + T \cdot \ln \left( 1 + \exp \left( -\frac{E + \tilde{\mu}}{T} \right) \right) \right], \quad (2.16)$$

with the energy  $E = \sqrt{k^2 + M^2}$ . Here the assumption is already made that the integral is spherical symmetric in momentum space, so it reduces to a one dimensional integral over  $k = |\vec{k}|$ . The latter part transforms with equations (2.13) and (2.14) to

$$G_S \langle \bar{\psi}\psi \rangle^2 = \frac{(M - m_0)^2}{4G_S}, \quad (2.17)$$

$$G_V \langle \psi^\dagger\psi \rangle^2 = \frac{(\mu - \tilde{\mu})^2}{4G_V}. \quad (2.18)$$

These equations are independent of space and time and the nucleon fields and therefore equation (2.10) is easy to evaluate for them. We are now able to formulate the thermodynamic potential for the Walecka model, from which all other thermodynamic observables can be derived. The full thermodynamic potential is given by

$$\Omega(T, \mu; M, \tilde{\mu}) = \omega_F(T, \mu; M, \tilde{\mu}) + \frac{(M - m_0)^2}{4G_S} - \frac{(\tilde{\mu} - \mu)^2}{4G_V}. \quad (2.19)$$

The shifted mass ( $M$ ) and the shifted chemical potential ( $\tilde{\mu}$ ) can be calculated via the following equations

$$\frac{\partial \Omega}{\partial M} = 0, \quad \frac{\partial \Omega}{\partial \tilde{\mu}} = 0, \quad (2.20)$$

as they are auxiliary variables and must not change the potential. This results in the gap equations

$$M = m_0 - \frac{4G_S}{\pi^2} \int_0^\infty dk \frac{k^2 \cdot M}{E} [n_- + n_+], \quad (2.21)$$

$$\tilde{\mu} = \mu - \frac{4G_V}{\pi^2} \int_0^\infty dk k^2 [n_- - n_+], \quad (2.22)$$

with the occupation numbers

$$n_\pm = \frac{1}{1 + \exp(-\frac{E \pm \tilde{\mu}}{T})}, \quad (2.23)$$

that describe a Fermi-Dirac distribution.

Now we are able to derive all thermodynamic properties of nuclear matter we are interested in, like the energy density  $\epsilon = \Omega(T, \mu; M, \tilde{\mu}) - \Omega(T, 0; M, 0) + \mu \cdot \rho$  or the baryon density  $\rho = -\frac{\partial \Omega}{\partial \mu}$

---

## 2.1 Limits for $T \rightarrow 0$

---

For the next part of the discussion we will need the zero temperature limits, which can be derived from (2.19)

$$\Omega(T = 0, \mu; M, \tilde{\mu}) = \omega_F(T = 0, \mu; \tilde{\mu}, M) + \frac{(M - m_0)^2}{4G_S} - \frac{(\mu - \tilde{\mu})^2}{4G_V}. \quad (2.24)$$

The free thermodynamic potential transforms to

$$\omega_F = -\frac{2}{\pi^2} \int dk k^2 \cdot (\tilde{\mu} - E) \theta(k_F - k). \quad (2.25)$$

Here the Fermi momentum is  $k_F = \sqrt{\tilde{\mu}^2 - M^2} \theta(\tilde{\mu}^2 - M^2)$ .

The shifted mass and chemical potential can be derived by taking the limit of (2.21) and (2.22) or by the conditions  $\frac{\partial \Omega}{\partial M}(T = 0, \mu; M, \tilde{\mu}) = 0$  and  $\frac{\partial \Omega}{\partial \tilde{\mu}}(T = 0, \mu; M, \tilde{\mu}) = 0$  and read

$$M = m_0 - \frac{4G_S}{\pi^2} \int dk k^2 \cdot \frac{M}{E} \theta(k_F - k), \quad (2.26)$$

$$\tilde{\mu} = \mu - \frac{4G_V}{\pi^2} \int dk k^2 \cdot \theta(k_F - k). \quad (2.27)$$

From the thermodynamic potential we can derive other thermodynamic observables. Of special interest here are the baryon density  $\rho$  and the energy density  $\epsilon$ , as they can be used to determine the coupling constants for known nuclear properties [Bub96]

$$\rho = \langle \psi^\dagger \psi \rangle = 4 \int \frac{d^3k}{(2\pi)^3} \theta(k_f - k) = \frac{2k_F}{3\pi^2}, \quad (2.28)$$

$$\epsilon = \Omega(T = 0, \mu; M, \tilde{\mu}) - \Omega(T = 0, \mu = 0; M, \tilde{\mu} = 0) + \mu \cdot \rho \quad (2.29)$$

$$= \frac{(M - m_0)^2}{4G_S} + \frac{(\mu - \tilde{\mu})^2}{4G_V} + \frac{2}{\pi^2} \int dk k^2 E \cdot \theta(k_F - k). \quad (2.30)$$

### 3 Determination of the Coupling Constants

To calculate the thermodynamic potential we have to determine the coupling constants  $g_\sigma$  and  $g_\omega$  as well as the exact meson masses  $m_\sigma$  and  $m_\omega$ . In equation (2.8) we can see, that those values only occur pairwise, so instead of determining four different values we can restrict ourselves to two parameters

$$\frac{g_\sigma}{m_\sigma}, \quad \frac{g_\omega}{m_\omega}. \quad (3.1)$$

So we need two conditional equations. These are taken from phenomenological data, like the binding energy [Gle96]

$$B/A = 16.3\text{MeV}, \quad (3.2)$$

at stable nuclear matter density  $\rho_0 = 0.17\text{fm}^{-3}$  [Bub96] and zero temperature. It is also well known that at this particular density the binding energy has to be minimal. This results in two equations for the two parameters

$$\left. \frac{\epsilon}{\rho} - m_0 \right|_{\rho=\rho_0} = -16.3\text{MeV}, \quad (3.3)$$

$$\left. \frac{d}{d\rho} \left( \frac{\epsilon}{\rho} \right) \right|_{\rho=\rho_0} = 0. \quad (3.4)$$

Here  $\epsilon$  is the energy density as described in chapter 2. These equations were solved using the Newton method with the results:

$$\frac{g_\sigma}{m_\sigma} = 0.018727 \frac{1}{\text{MeV}}, \quad (3.5)$$

$$\frac{g_\omega}{m_\omega} = 0.016219 \frac{1}{\text{MeV}}. \quad (3.6)$$

In figure 3.1 we can see, that with the aforementioned coupling constants the two given properties of nuclear matter are reproduced very well.

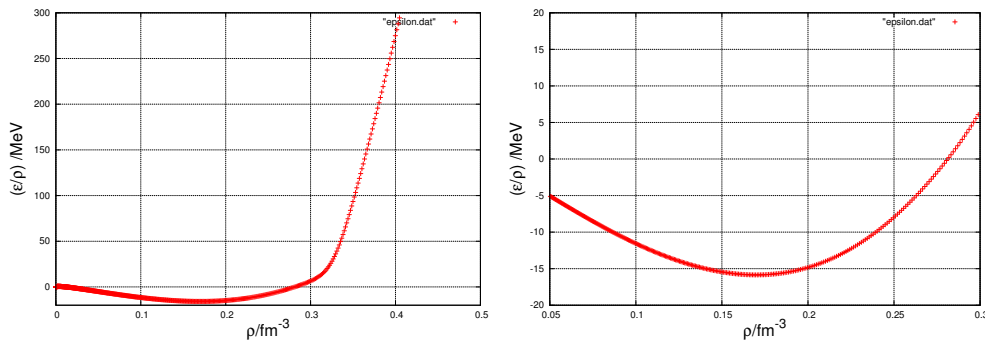


**Figure 3.1:** Energy density over nucleon density with the calculated coupling constants at different scales left and right.

## 4 Homogeneous Phase Diagram

We are now ready to calculate the thermodynamic potential and all other observables. This leads to a phase diagram for nuclear matter. The effective mass of the nucleons changes with varying chemical potentials and temperatures. At low chemical potentials the nucleons behave like free particles and their effective mass is the free nucleon masses. With increasing chemical potential at low temperature the effective mass is lower because the nucleons get into bound states and are better described in the liquid drop model. This happens suddenly, this means there is a first order phase transition in nuclear matter. To determine the phase diagram we take a look at the thermodynamic potential as a function of

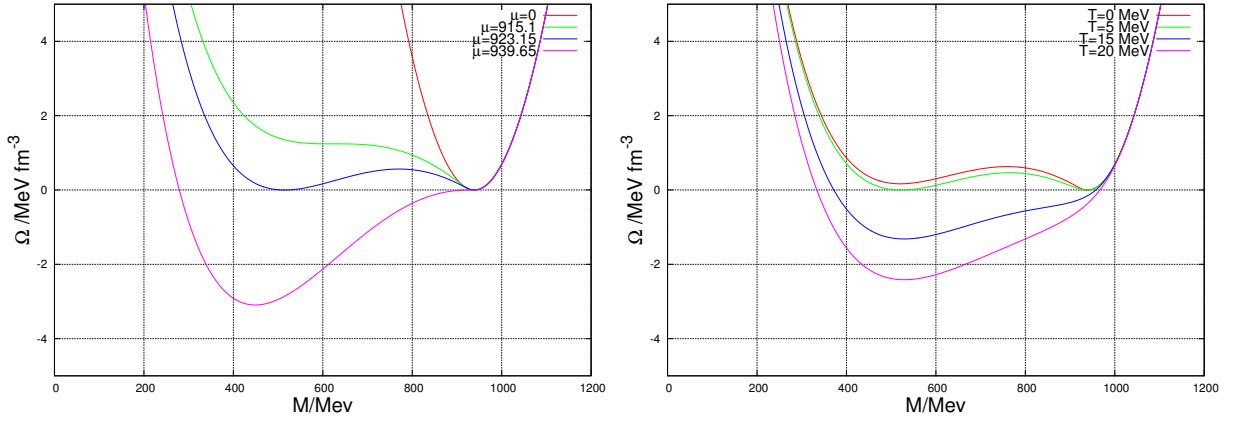


**Figure 4.1:** The thermodynamic potential  $\Omega$  over the shifted mass  $M$  for different chemical potentials  $\mu$  at  $T = 0$  (left) and for different  $T$  at  $\mu = 922.155$  MeV (right)

the effective mass (figure 4.1). The thermodynamic potential has to be minimal, but there are different extremal solutions. At the phase transition the two minima are in equilibrium, bound and free states coexist, but at different  $\mu$  or  $T$  there is only one minimal solution. Analyzing figure 4.1, we can see that at lower  $\mu$  and  $T$  the free nucleon mass is the minimal solution, but at high  $\mu$  and  $T$  the minimum at lower effective masses is the minimal solution. This results in a sudden drop of the effective mass, as can be seen in figure 4.3. At high enough temperatures there is no phase transition anymore, only one continuously shifting minimum. This is what happens in the  $T = 200$  MeV case in figure 4.3. The end point is also called critical point. Converging to this point the maximum that can be seen in figure 4.1 is approaching the same energy as the two minima, which results in a small plateau. We can now calculate the phase diagram (figure 4.2) with the critical point at

$$\mu_C = 910.143 \text{ MeV}, \quad T_C = 19.263 \text{ MeV}. \quad (4.1)$$

For later discussions it is useful to introduce the phase diagram for nuclear matter without vector interaction. This has no physical significance, but from the discussion of inhomogeneous phases in the NJL model [CNB10] we expect the end point of the inhomogeneous phases, for the case with and without vector interaction, to be at the same temperature as the critical point of the homogeneous phase transition without vector interaction. In figure 4.2 we can see, that there is no end point in the phase diagram, even at  $\mu = 0$  there is a clear transition. It shows the expected behavior that the transition line is much longer and the starting point at  $T = 0$  is shifted to lower chemical potentials. The grand canonical potential looks similar to figure 4.1 and the method to determine the phase transition is the same.

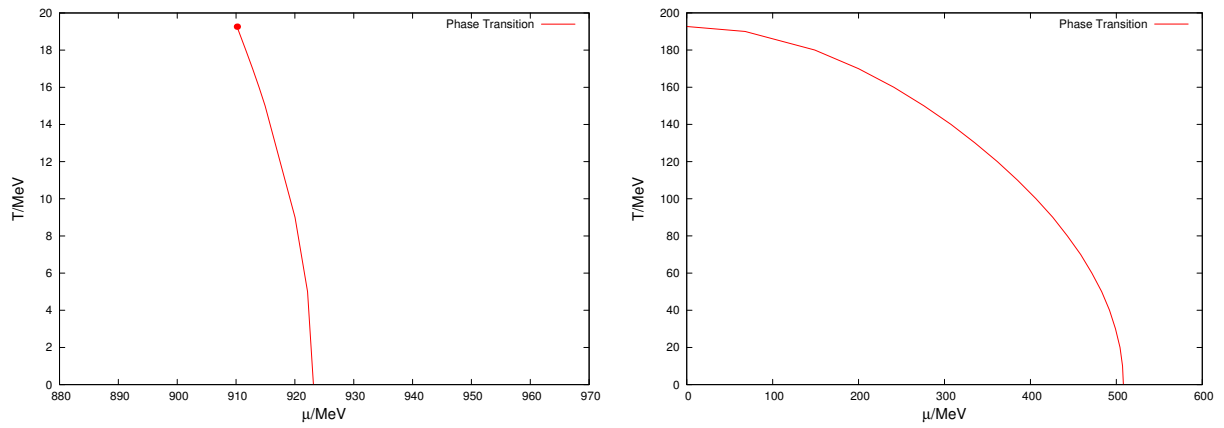


**Figure 4.2:** Phase transition in nuclear matter with full vector coupling (left) and no vector coupling (right)

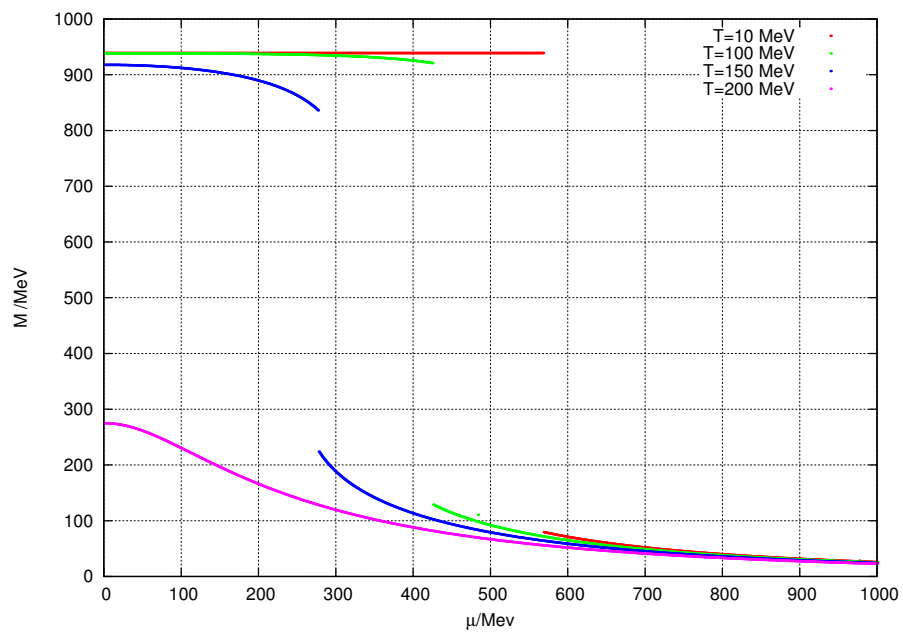


**Figure 4.3:** Effective mass  $M$  over  $\mu$  at different Temperatures and  $G_V=0$ .

---

## 5 Inhomogeneous Phase

---

In the discussions above we considered mean fields as an approximation for the mesonic fields. Those mean values were space and time independent. One possible generalization would be to allow spatially varying fields. In order to do this we take the NJL type Lagrangian for the Walecka model

$$\mathcal{L} = \bar{\psi}(i\gamma^\mu \partial_\mu - m_0)\psi + G_S (\bar{\psi}\psi)^2 - G_V (\bar{\psi}\gamma^\mu\psi)^2. \quad (5.1)$$

We then replace the fields by spatially dependent arbitrary functions and neglect quadratic contributions[CNB10]

$$(\bar{\psi}\psi)^2 = -S(x)^2 + 2S(x)(\bar{\psi}\psi), \quad (5.2)$$

$$(\bar{\psi}\gamma^\mu\psi)^2 = -n(x)^2 + 2n(x)\bar{\psi}\gamma^0\psi. \quad (5.3)$$

Again we define a shifted mass and chemical potential in the following way

$$M(x) = m_0 - 2G_S S(x), \quad (5.4)$$

$$\tilde{\mu} = \mu - 2G_V n(x). \quad (5.5)$$

We approximate the nucleon density  $n(x)$  by its spatial average

$$n(x) \rightarrow \langle n(x) \rangle \doteq \bar{n}. \quad (5.6)$$

In the case for a constant density the solution for the mass is similar to the results from the 1+1 dimensional Gross-Neveu-Model [STU06] and is an oscillating function. The exact derivation of the grand canonical potential and the different equations would exceed the frame of this thesis and can be found in [Nic09] and [CNB10]. The results are given in the section below.

---

### 5.1 Grand Canonical Potential

---

We start from the mass, as it is the most important change of the model in this section

$$M(z) = \Delta \left( v \operatorname{sn}(b|v) \operatorname{sn}(\Delta z|v) \operatorname{sn}(\Delta z + b|v) + \frac{\operatorname{cn}(b|v) \operatorname{dn}(b|v)}{\operatorname{sn}(b|v)} \right). \quad (5.7)$$

The effective mass is an oscillating function dependent on a one dimensional space parameter  $z$  and three auxiliary parameters  $\Delta$ ,  $v$  and  $b$  in terms of which the grand canonical potential has to be minimized.  $\operatorname{sn}(u|k)$ ,  $\operatorname{cn}(u|k)$  and  $\operatorname{dn}(u|k)$  represent the Jacobi elliptic functions. The grand canonical potential now looks like this

$$\Omega = -2 \cdot \int_0^\infty dE \rho(E) f_{medium}(\sqrt{E^2 + \delta \Delta^2}) + \frac{1}{L} \int_0^L dz \left( \frac{|M(z) - m_0|^2}{4G_S} - \frac{(\tilde{\mu} - \mu)^2}{4G_V} \right), \quad (5.8)$$

with the density of states  $\rho(E)$ , the shifted mass  $M(z)$  and chemical potential  $\tilde{\mu}$ , the period of the oscillation  $L = 2\mathbf{K}(v)/\Delta$  and

$$f_{medium}(x) = T \cdot \left[ \ln \left( 1 + \exp \left( -\frac{x - \tilde{\mu}}{T} \right) \right) + \ln \left( 1 + \exp \left( -\frac{x + \tilde{\mu}}{T} \right) \right) \right]. \quad (5.9)$$

We have also introduced the substitution  $\delta = 1/\text{sn}^2(b|\nu) - 1$ . The density of states reads

$$\begin{aligned} \rho(E) = & \frac{E\Delta}{\pi^2} \left( \theta(\sqrt{\tilde{\nu}}\Delta - E) \left[ \mathbf{E}(\tilde{\theta}|\tilde{\nu}) + \left( \frac{\mathbf{E}(\nu)}{\mathbf{K}(\nu)} - 1 \right) \mathbf{F}(\tilde{\theta}|\tilde{\nu}) \right] \right. \\ & + \theta(E - \sqrt{\tilde{\nu}}\Delta)\theta(\Delta - E) \left[ \mathbf{E}(\tilde{\nu}) + \left( \frac{\mathbf{E}(\nu)}{\mathbf{K}(\nu)} - 1 \right) \mathbf{K}(\tilde{\nu}) \right] \\ & \left. + \theta(E - \Delta) \left[ \mathbf{E}(\theta|\tilde{\nu}) + \left( \frac{\mathbf{E}(\nu)}{\mathbf{K}(\nu)} - 1 \right) \mathbf{F}(\theta|\tilde{\nu}) + \frac{\sqrt{(E^2 - \Delta^2)(E^2 - \tilde{\nu}\Delta^2)}}{(E\Delta)} \right] \right), \end{aligned} \quad (5.10)$$

where  $\mathbf{K}(k)$  and  $\mathbf{E}(k)$  denote the complete elliptic integrals of first and second kind,  $\mathbf{F}(\phi|k)$  and  $\mathbf{E}(\phi|k)$  the incomplete elliptic integrals of first and second kind and  $\tilde{\nu} = 1 - \nu$ ,  $\theta = \arcsin(\Delta/E)$ ,  $\tilde{\theta} = \arcsin(E/(\sqrt{\tilde{\nu}}\Delta))$ .

The effective chemical potential in equation (5.5) is a self consistent function depending on the nuclear density  $\bar{n}$ , which is given in terms of the density of states  $\rho(E)$

$$\bar{n} = 2 \int_0^\infty dE \rho(E) \left( n_+(\sqrt{E^2 + \delta\Delta^2}) - n_-(\sqrt{E^2 + \delta\Delta^2}) \right), \quad (5.11)$$

and the occupation numbers

$$n_\pm(x) = \frac{1}{1 + e^{\frac{x \mp \mu}{T}}}. \quad (5.12)$$

The grand canonical potential has now to be minimized in terms of the parameters  $\Delta$ ,  $\nu$  and  $b$ . The order parameter in this theory is  $M$ , so to see a phase transition from homogeneous to inhomogeneous phases we have to look at the linear and quadratic expectation values

$$\langle M(z) \rangle = \frac{1}{L} \int_0^L dz M(z), \quad (5.13)$$

$$\langle M(z)^2 \rangle = \frac{1}{L} \int_0^L dz (M(z))^2. \quad (5.14)$$

This can be done by direct integration of equation (5.7) or via the following relations

$$\langle M(z) \rangle = \Delta \cdot \left[ \mathbf{Z}(b|\nu) + \frac{\text{cn}(b|\nu)\text{dn}(b|\nu)}{\text{sn}(b|\nu)} \right], \quad (5.15)$$

$$\langle M(z)^2 \rangle = \Delta^2 \cdot \left[ \frac{1}{\text{sn}^2(b|\nu)} + 1 - \nu - 2 \frac{\mathbf{E}(\nu)}{\mathbf{K}(\nu)} \right], \quad (5.16)$$

where  $\mathbf{Z}(b|\nu)$  denotes the Jacobi Zeta function in terms of the Jacobi Amplitude of  $b$  and  $\nu$ . If the square root of the quadratic expectation value and the linear expectation value differ, we are in an inhomogeneous phase.

---

### 5.1.1 Limits

---

It is important for numerical calculations as well as for a better grasp of the theory to know the limits in  $\nu$  for the aforementioned equations, because they represent the transition to homogeneous phases. To see the behavior of the elliptic functions we plotted the mass in the limits  $\nu \rightarrow 0$  and  $\nu \rightarrow 1$  for arbitrary values of  $\Delta$  and  $b$  in figure 5.1. The mass limits are the following

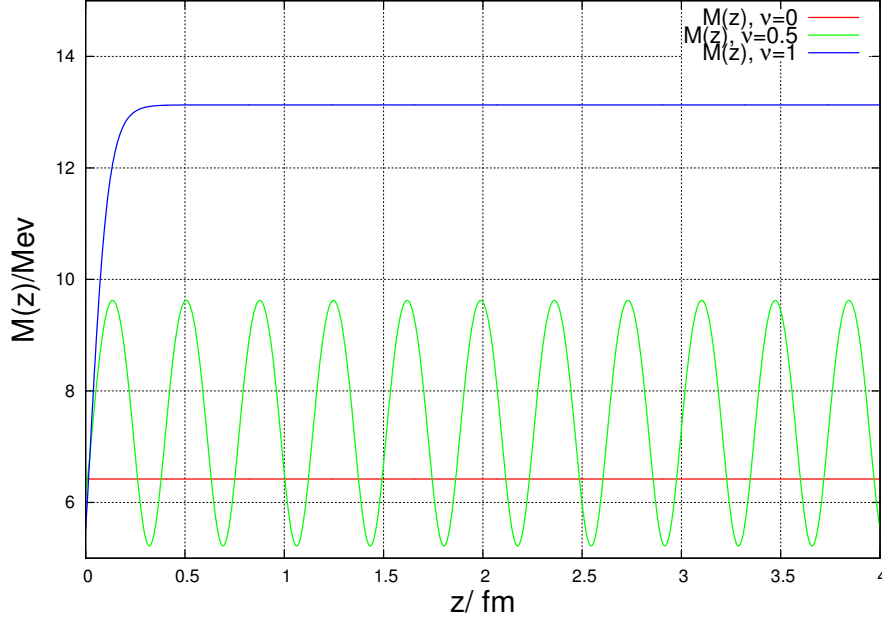


**Figure 5.1:** The effective mass  $M(z)$  over  $z$  for different values of  $\nu$  with  $\Delta = 10$  and  $b = 1$

$$\lim_{\nu \rightarrow 0} M(z) = \Delta \cdot \cot(b), \quad (5.17)$$

$$\lim_{\nu \rightarrow 1} M(z) = \Delta \cdot [\coth(b) + \tanh(\Delta \cdot z) - \tanh(\Delta \cdot z + b)]. \quad (5.18)$$

We can see that for very low  $\nu$  the mass is a constant in space and shows no oscillation. With increasing  $\nu$  the mass starts oscillating with a period  $\frac{2 \cdot K(\nu)}{\Delta}$  until in the  $\nu = 1$  case it transforms to a hyperbolic tangent, which means small changes at low distance, but it is asymptotically constant.

We also calculate the limits for the expectation values of the mass:

$$\lim_{\nu \rightarrow 0} \langle M \rangle = \frac{\Delta}{\tan(b)}, \quad (5.19)$$

$$\lim_{\nu \rightarrow 1} \langle M \rangle = \frac{\Delta}{\tanh(b)}, \quad (5.20)$$

$$\lim_{\nu \rightarrow 0} \langle M^2 \rangle = \frac{\Delta^2}{\tan^2(b)}, \quad (5.21)$$

$$\lim_{\nu \rightarrow 1} \langle M^2 \rangle = \frac{\Delta^2}{\tanh^2(b)}. \quad (5.22)$$

As mentioned before, the expectation values are an indicator for inhomogeneous phases, and it can easily be seen that  $\sqrt{\langle M^2 \rangle} = \langle M \rangle$  in the limits, so the limits always represent homogeneous phases.

For numerical calculations it is also important to derive the limits for the density of states

$$\lim_{\nu \rightarrow 0} \rho(E) = \frac{E^2}{\pi^2}, \quad (5.23)$$

$$\lim_{\nu \rightarrow 1} \rho(E) = \frac{\sqrt{E^2 - \Delta^2} \cdot E}{\pi^2} \theta(E - \Delta). \quad (5.24)$$

With these relations we are able to do examine the Walecka model for inhomogeneous phases.

## 6 Phase Diagram with Inhomogeneous Phases

Now we have the tools to examine inhomogeneous dense nuclear matter. To simplify numerical calculations we express the the integral over the mass differently than in equation (5.8)

$$\frac{1}{L} \int_0^L dz |M(z) - m_0|^2 = \frac{1}{L} \int_0^L dz (\langle M(z)^2 \rangle - 2m_0 \langle M(z) \rangle + m_0^2). \quad (6.1)$$

The integrand is now independent of  $z$ , so we can neglect the integration and get

$$\frac{1}{L} \int_0^L dz |M(z) - m_0|^2 = \langle M(z)^2 \rangle - 2m_0 \langle M(z) \rangle + m_0^2. \quad (6.2)$$

The potential is minimized for every  $T$  and  $\mu$  in terms of  $\Delta$ ,  $\nu$  and  $b$  by applying the simplex algorithm of Nelder and Mead integrated in the GSL.

We start the discussion concentrating on the case without vector interaction. One of the indicators for inhomogeneous phases is that the linear and the square root of the quadratic expectation values differ. We have seen in section 5.1.1 that the expectation values have to be the same in the limits for  $\nu \rightarrow 0$  and  $\nu \rightarrow 1$ , so differing expectation values indicate an oscillation of the effective mass.

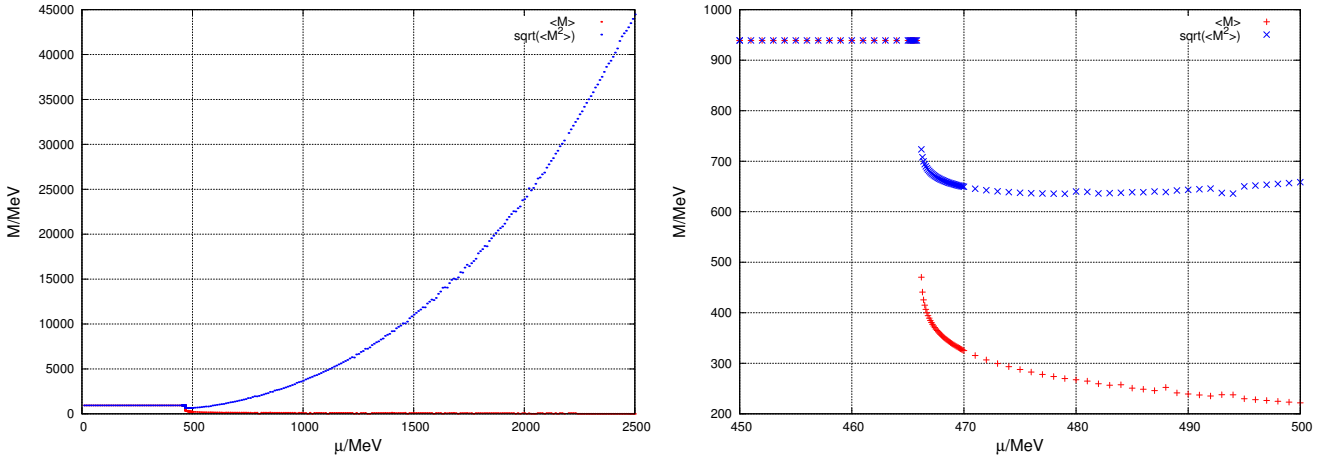


**Figure 6.1:** The expectation values of the effective mass at  $T = 10$  MeV on a large scale (left) and a small scale close to the transition to inhomogeneous phases (right).

In figure 6.1 we have plotted the linear and the square root of the quadratic expectation value over the chemical potential. At  $\mu = 466$  MeV we can see that both expectation values drop and start to differ. With increasing chemical potential the quadratic expectation value  $\sqrt{\langle M^2 \rangle}$  is growing very fast, while the linear expectation value  $\langle M \rangle$  is dropping slowly. In the NJL model the phase becomes homogeneous again at higher  $\mu$ , this behavior cannot be reproduced in the Walecka model. Even at very high chemical potentials, like  $\mu \approx 7000$  MeV, we are still in an inhomogeneous phase. This enables us to draw a phase diagram with a line where the inhomogeneous phase starts, but there is no end as far as we can tell. We see that the phase transition for low temperatures starts at a chemical potential roughly 50 MeV lower than the homogeneous transition and joins the homogeneous transition at higher temperatures. With the precision of  $\Delta\mu = 1$  MeV used in this calculations the point from where both lines are equal is at  $\mu = 200$  MeV.

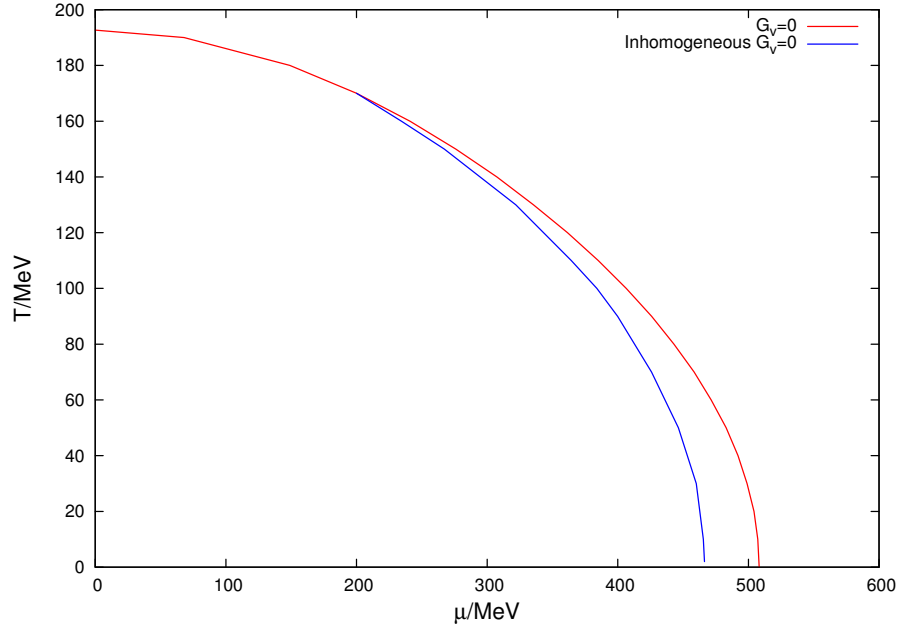


**Figure 6.2:** Phase diagram of nuclear matter with the transition to inhomogeneous phases (blue line) and the homogeneous phase transition (red line) without vector coupling.

The effective mass near the phase transition can be seen in figure 6.3. At low chemical potentials it is a constant in space and equals the free nucleon mass, from the knowledge of the limits discussed in chapter 5.1.1 this is what we expected for  $\nu \rightarrow 0$ . For higher chemical potentials  $\mu = 500$  MeV the mass starts oscillating in space. We should note here that this is before the homogeneous phase transition found in chapter 4. Although the effective mass has negative values it can easily be seen that it has a positive average. With rising  $\mu$  the oscillation has a bigger amplitude and a shorter period. The average is smaller, the mass has a bigger negative contribution.

Now we are able to understand the difference of the linear and the quadratic expectation values, the positive and the negative amplitude approach with rising  $\mu$  and therefore the average tends to zero. The absolute amplitude is increasing, this means the quadratic expectation values increases as well, as there is no negative contribution.

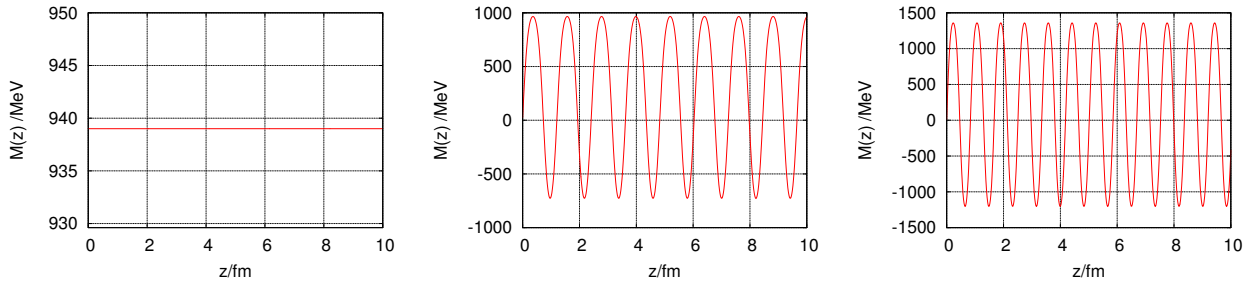


**Figure 6.3:** The effective mass  $M(z)$  over  $z$  for  $\mu = 400$  MeV (left),  $\mu = 500$  MeV (center) and  $\mu = 600$  MeV (right).

Now we take a look at the average density shown in figure 6.4. As expected the density equals roughly zero at low temperatures and low chemical potentials. For very high  $\mu$  the density grows steadily to very high values. At the inhomogeneous phase transition the density grows very quickly, within the achieved precision we are not able to tell, whether it is a continuous transition or there is a jump in the density. Given the similarities between to the density profile found in the NJL model in [CNB10], the average density is likely to be continuous.

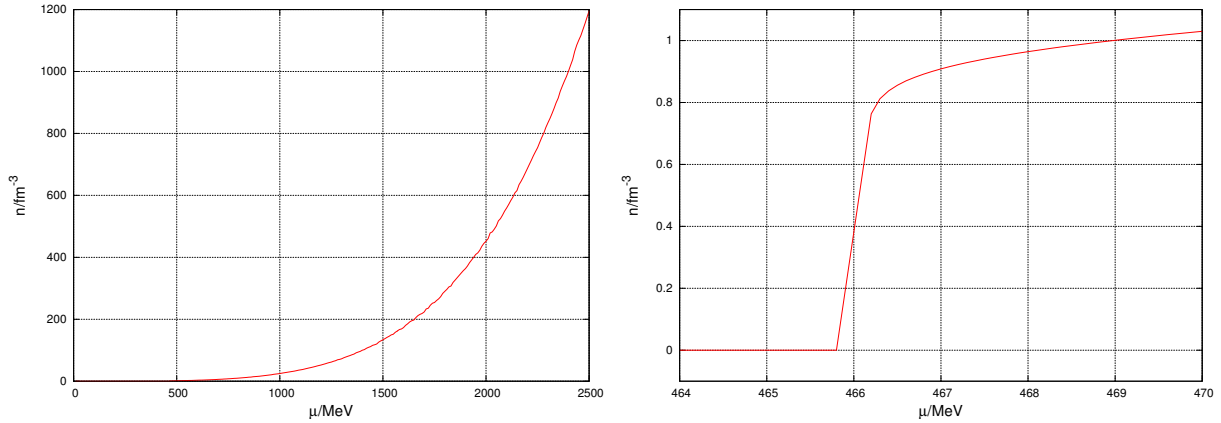


**Figure 6.4:** The average density as a function of the chemical potential at  $T = 10$  MeV on a large scale (left) and a small scale close to the transition to inhomogeneous phases (right)

All discussions above were for the case without vector interaction. The calculations with vector coupling were much more complicated and required more time. For every step in the minimizer the shifted chemical potential has to be calculated from the self consistent equation (5.5). The minimization of the thermodynamic potential was very unstable, we got different results for slightly different starting values, which made it very difficult to find the global minimum. It was not possible to do the necessary calculations in the given time for this thesis. All we can do is a qualitative discussion.

We know that the starting point of inhomogeneous phases at  $T = 0$  has to be the same for the case with and without vector interaction, because the density is zero at this point, which means that  $\mu = \tilde{\mu}$  there. For high  $\mu$  we would expect a similar behavior as seen in without vector interaction. The shifted chemical potential grows slower than the normal chemical potential, so we cannot expect the inhomogeneous phases to end within the calculated ranges. For the same reason the inhomogeneous phases for higher temperatures are likely to start at higher  $\mu$  compared to the case without vector interaction. If plotted over the shifted chemical potential  $\tilde{\mu}$  the transition line for inhomogeneous phases should look identically to figure 6.2.

---

## 7 Conclusion and Outlook

---

We started with the Walecka Lagrangian for nuclear matter. Then we derived the grand canonical potential for finite temperatures in a mean field approximation and its limits for  $T = 0$ . We calculated the coupling constants for the model by adjusting them to known properties of nuclear matter. This enabled us to draw a phase diagram with the critical point  $\mu_C = 910.143 \text{ MeV}$ ,  $T = 19.263 \text{ MeV}$ . We were also able to derive other thermodynamic observables and understood the presence of a first order phase transition in nuclear matter by examination of the thermodynamic potential. Then we extended the model by allowing spatially dependent functions instead of mean fields for the mesons. This led to inhomogeneous phases with oscillating masses. We examined the phase diagram for the case without vector interaction and found inhomogeneous phases to be present in the Walecka model. We have drawn a phase diagram for the inhomogeneous phases and analyzed the effective mass and the average density. Problems occurred when we tried to allow vector interaction, the minimal solutions for the thermodynamic potential got very unstable, small changes in the starting values led to dramatic changes in the results. We can only note that in principle it is possible to find inhomogeneous phases in the Walecka model with full vector couplings, but it demands very time intensive calculations, that would have exceeded the given time frame of this thesis.

It is also noteworthy, that we started from a NJL type Lagrangian, which looks very similar to the Lagrangian in the Walecka model in mean field approximation, but if we introduce the spatially dependent functions in the Euler-Lagrange equations, there might be different results.

The Walecka model uses no meson self interactions, but it is possible to get a better description of nuclear matter if these self interactions are introduced. For example the compressibility of nuclear matter is reproduced more accurately with  $\sigma$ -meson self interaction.

---

## List of Figures

---

3.1	Energy density over nucleon density with the calculated coupling constants at different scales left and right. . . . .	8
4.1	The thermodynamic potential $\Omega$ over the shifted mass $M$ for different chemical potentials $\mu$ at $T = 0$ (left) and for different $T$ at $\mu = 922.155$ MeV (right) . . . . .	9
4.2	Phase transition in nuclear matter with full vector coupling (left) and no vector coupling (right) . . . . .	10
4.3	Effective mass $M$ over $\mu$ at different Temperatures and $G_V = 0$ . . . . .	10
5.1	The effective mass $M(z)$ over $z$ for different values of $\nu$ with $\Delta = 10$ and $b = 1$ . . . . .	13
6.1	The expectation values of the effective mass at $T = 10$ MeV on a large scale (left) and a small scale close to the transition to inhomogeneous phases (right). . . . .	14
6.2	Phase diagram of nuclear matter with the transition to inhomogeneous phases (blue line) and the homogeneous phase transition (red line) without vector coupling. . . . .	15
6.3	The effective mass $M(z)$ over $z$ for $\mu = 400$ MeV (left), $\mu = 500$ MeV (center) and $\mu = 600$ MeV (right). . . . .	15
6.4	The average density as a function of the chemical potential at $T = 10$ MeV on a large scale (left) and a small scale close to the transition to inhomogeneous phases (right) . . . . .	16

---

## Bibliography

---

- [Bub96] Michael Buballa. The problem of matter stability in the Nambu-Jona-Lasinio model. *Nucl. Phys.*, A611:393–408, 1996.
- [CNB10] Stefano Carignano, Dominik Nickel, and Michael Buballa. Influence of vector interaction and Polyakov loop dynamics on inhomogeneous chiral symmetry breaking phases. *Phys. Rev.*, D82:054009, 2010.
- [Gle96] Norman Glendenning. *Compact Stars*. Springer, 1996.
- [Kap05] Kapusta. *Finite Temperature Field Theory*. Cambridge University Press, 2005.
- [N<sup>+</sup>10] K Nakamura et al. Review of particle physics. *J. Phys.*, G37:075021, 2010.
- [Nic09] Dominik Nickel. Inhomogeneous phases in the Nambu-Jona-Lasino and quark- meson model. *Phys. Rev.*, D80:074025, 2009.
- [Sch07] David Scheffler. NJL model study of the QCD phase diagram using the Taylor series expansion technique. *Bachelor Thesis*, 2007.
- [STU06] Oliver Schnetz, Michael Thies, and Konrad Urlich. Full phase diagram of the massive Gross-Neveu model. *Annals Phys.*, 321:2604–2637, 2006.
- [Wal74] J. D. Walecka. A theory of highly condensed matter. *Annals Phys.*, 83:491–529, 1974.